Composites Part A 109 (2018) 472–480

Contents lists available at ScienceDirect

Composites Part A

journal homepage: www.elsevier.com/locate/compositesa

Multifunctional anisotropic flexible cycloaliphatic epoxy resin nanocomposites reinforced by aligned graphite flake with non-covalent biomimetic functionalization

Zheng Su[a,b], Hua Wang[a,c,*], Konghu Tian[a,b], Weiqi Huang[a,b], Yulan Guo[a,b], Jing He[a,b], Xingyou Tian[a,c,**]

[a] Institute of Applied Technology, Hefei Institutes of Physical Science, Chinese Academy of Sciences, Hefei 230031, PR China
[b] University of Science and Technology of China, Hefei 230036, PR China
[c] Key Laboratory of Photovoltaic and Energy Conservation Materials, Chinese Academy of Sciences, PR China

ARTICLE INFO

Keywords:
Polymer-matrix composites (PMCs)
Anisotropy
Thermal properties
Adhesive

ABSTRACT

High thermal conductive filler (graphite flake) reinforced polymer composites have obtained a growing attention in the microelectronic industry. In order to overcome the obstacles in surface modification, in this study, dopamine chemistry was used to achieve the facile modification of graphite flake via forming a polydopamine (PDA) shell on the surface in a solvent-free aqueous condition. The strong π-π interaction between the hexagonal structural graphite flake and aromatic dopamine molecules ensured the effective modification. The PDA coating on graphite flake enhanced the compatibility between the filler and the flexible cycloaliphatic epoxy resin (CER) matrix via hydrogen bond, and promoted the epoxy curing process by forming covalent bond. Under the assistance of gravity, the PDA@graphite flake stacked along the horizontal direction in the polymer matrix. The procedure of filler alignment and mechanism of thermal decomposition were investigated by XRD measurement and thermodynamic/kinetics analysis, respectively. The dynamic mechanical analysis (DMA) was also used to investigate the relationship between microstructure and performance. Due to the combination of surface modification and alignment of PDA@graphite flake, the prepared CER/PDA@graphite has higher in-plane thermal conductivity. In addition, excellent adhesion property and thermal stability demonstrated that the CER/PDA@graphite composites was a good candidate as thermal interface material (TIMs), which could be applied in the thermal management areas. The procedure was environment friendly, easy operation, and suitable for the practical application in large scale.

1. Introduction

Next-generation processer is running faster and faster, however, with the higher energy consumption and accumulation. There is necessary to investigate the higher thermal conductivity materials to meet the specification of low energy consumption devices and prevent the heat accumulation in the microelectronic industry. Thermal interface materials (TIMs) are applied between heat sources and heat sinks, which were essential ingredients of thermal management [1,2]. Currently, TIMs are mainly based on polymer, greases, and adhesives filled with thermal conductive filler such as alumina, silica, or silver, which requires high volume fraction (~50–70 vol%) to achieve thermal conductivity in the range of 1–5 W/m·K at room temperature [3]. In addition, a number of carbon-materials had been used to improve the thermal conductivity of polymer-matrix composites as TIMs. Carbon nanotubes (CNTs, ~3000 W/m·K along the tube axis) and graphene sheets (~5000 W/m·K along the x-y plane) had emerged as an efficient filler due to their high thermal conductivity and high aspect ratio, however, not led to practical application due to the weak thermal coupling between filler/base interface and prohibitive cost [4,5].

The graphite flake is a kind of 2D materials with high aspect ratio, which contains monolayer or few to hundreds of stacked graphene layers. The high in–plane thermal conductivity of graphite (2000 W/m·K) has more important application in heat dissipation [6,7]. Especially for their low thermal contact resistance of ultrathin and flexible graphite and graphene flakes, which are the promising candidates for TIMs [8]. They are expected to form a very efficient heat conduction pathway in polymer matrix [9,10].

* Corresponding author at: Institute of Applied Technology, Hefei Institutes of Physical Science, Chinese Academy of Sciences, Hefei 230031, PR China.
** Corresponding author at: Institute of Applied Technology, Hefei Institutes of Physical Science, Chinese Academy of Sciences, Hefei 230031, PR China.
E-mail addresses: wanghua@issp.ac.cn (H. Wang), xytian@issp.ac.cn (X. Tian).

https://doi.org/10.1016/j.compositesa.2018.02.033
Received 26 November 2017; Received in revised form 27 January 2018; Accepted 22 February 2018
Available online 23 February 2018
1359-835X/

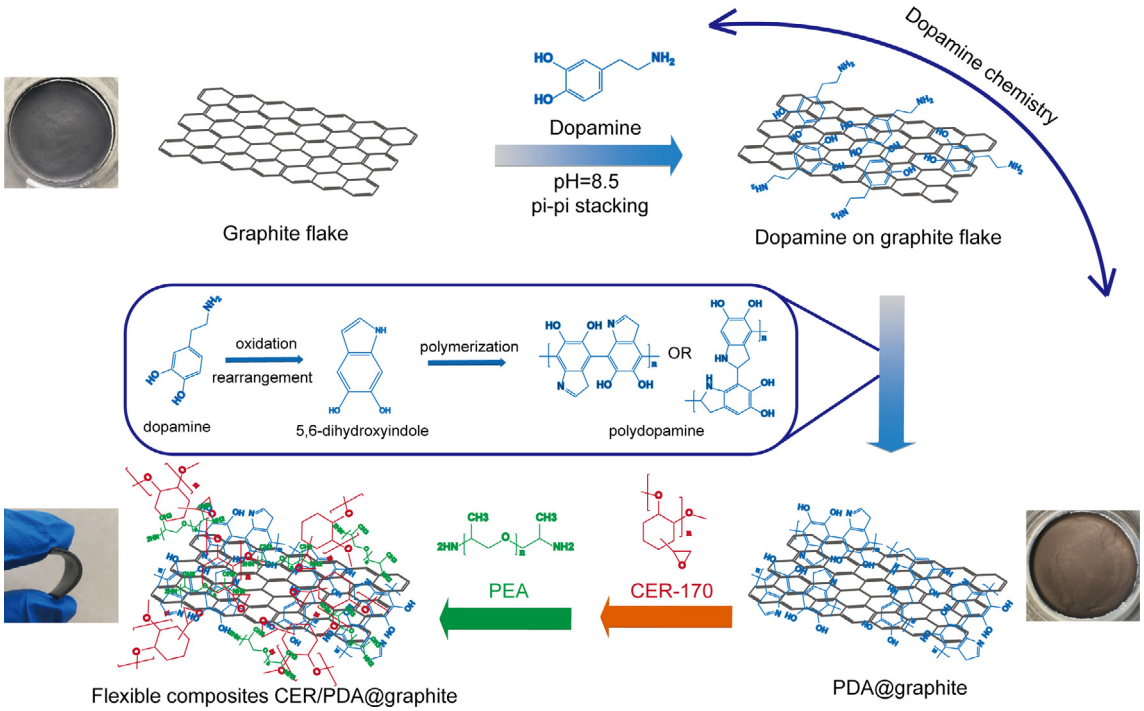

Fig. 1. Schematic illustration of the procedure to prepare the flexible composites CER/PDA@graphite. (For interpretation of the references to colour in this figure legend, the reader is referred to the web version of this article.)

The interface thermal resistance between filler and matrix would also affect the thermal conductivity properties significantly. Surface modification of filler had been demonstrated to be an efficient way to improve the miscibility and affinity with polymers, which was benefit to increase the thermal conductivity of the composites [11,12]. Yu et al. modified the BN nano-platelets through noncovalent functionalization by octadecylamine (ODA) and covalent functionalization by hyperbranched aromatic polyamide (HBP) to obtain a strong interface between filler and polymer matrix and thermal conductivity could arrive at 0.28 W/m·K at around room temperature [13]. Peng et al. used gamma-aminopropyl triethoxysilane (KH550) as the silane coupling agent for the surface modification of the AlN nanoparticles which improved the dispersion of the nanoparticles in epoxy resin and obtained best value of thermal conductivity was 0.42 W/m·K at 20 °C [14]. Yu et al. intercalated and exfoliated the natural graphite in acetone to prepare graphite nano-platelets of controlled aspect ratio [15]. They found that the graphite nano-platelets with high aspect ratio would enhanced the thermal conductivity of the polymer composites significantly. However, most chemical modifications were very laborious and involved the use of solvents, which might cause environmental issues. Especially for the covalent bond functionalization which would destroy the lattice structure of filler and then affect the heat transformation according to the phonon mean free path theory of thermal conductivity [16,17]. Therefore, it was essential to find an easy and environment-friendly method for processing and functionalization of graphite flake without much loss of heat transfer performance.

In this work, dopamine chemistry was applied to functionalize the commercial graphite flake, which was inspired by the adhesive protein polydopamine, found in the anchoring mechanism of mussels. Dopamine was widely used in surface functionalization, which was easily oxidized to self-polymerize into polydopamine (PDA). Because of the aromatic structure of polydopamine in alkaline aqueous solution, the PDA molecule can coat on almost all kinds of substrates especially for hexagonal structure (such as BN, CNT, graphene) via π-π and van der Waals interaction [18,19]. This bioinspired method was regard as an easy and green surface modification method because of its room temperature reaction and no harmful solvents involved. Cycloaliphatic Epoxy Resin (CER-170) was chosen as the matrix for their adhesion and flexibility. Herein, the morphology, thermal conductivity, thermal stability, mechanical, and adhesive property of the composites were studied respectively. The XRD measurement was used to investigate the aligned structure and mechanism of composites by calculating the orientation degree. An interesting phenomenon was found in the analysis of thermal stability property when compared the integral procedural decomposition temperature (IPDT) and activation energy (E_t). Graphite flake was modified by PDA, and the resulted product PDA@graphite could be easily dispersed in polymer matrix with aligned structure. The obtained thermal conductivity was high enough (~9.053 W/m·K) at in-plane direction with excellent adhesive properties. The resulting indicated the promising prospect in the area of thermal management.

2. Experimental section

2.1. Materials

Graphite flake was purchased from Qingdao Huatai Lubricant Sealing S&T Co., Ltd. Dopamine hydrochloride (98%), tris(hydroxymethyl) aminomethane (Tris, ≥99.9%) were obtained from Aladdin. Cycloaliphatic epoxy (CER-170) was obtained from Wuhan Sen Mao Fine Chemical Co., Ltd. Polyetheramine (PEA, BASF EC 301) as curing agent from BASF SE. For all experiments, deionized water was used.

2.2. Surface modification of graphite flake

The graphite flake of 5 g was dispersed in the mixed solution of 750 mL of Tris-buffer solution (10 mM, pH 8.5) and 2.5 g ethanol, and then 1.5 g dopamine hydrochloride was added. After ultrasonic treatment for 1 h, the mixture was stirred at room temperature for 24 h. After that reaction, the modified graphite flake powder, coded as PDA@graphite which was centrifuged and washed by deionized water and ethanol for several times before being dried at 65 °C.

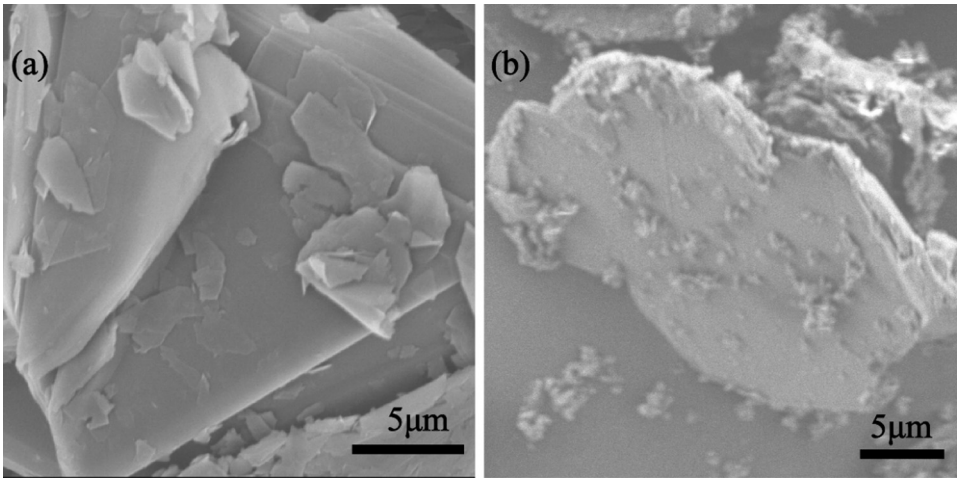

Fig. 2. SEM images of (a) pristine and (b) dopamine-treated graphite flake.

2.3. Preparation of the cycloaliphatic epoxy resin/PDA@graphite composite film

Monoliths of cycloaliphatic epoxy resin (CER)/PDA@graphite composites were prepared as follows: epoxy resin (cycloaliphatic epoxy resin, CER 170) was added to the Teflon beaker and then the curing agent (polyetheramine, PEA BASF EC 301) was added with continuous stirring. After 10 min high-shear mixing, various amount of PDA@graphite was added with continuous stirring at high speed for 2 h. The mixture of cycloaliphatic epoxy with the aligned PDA@graphite was coated on the silicone oil paper at room temperature for curing few days. A serious of composites were prepared with loading of PDA@graphite at 10 wt%, 30 wt% and 50 wt%. Fig. 1 showed schematic illustration of the procedure to prepare the flexible composites CER/PDA@graphite.

2.4. Characterizations techniques

X-ray film and powder diffraction (XRD) patterns were carried on a Philips X'Pert Pro MPD X-ray diffractometer (40 kV, 40 mA) with Cu-Ka radiation (λ = 0.154 nm). Raman spectra of samples were measured using a Confocal Raman Microscopy (Renishaw inVia Reflex) with an excitation wavelength of 514.5 nm. Infrared (IR) test was carried out on a Nicolet 8700 FTIR spectrometer (Thermo Scientific Instrument Co. USA) using KBr pellet method. The morphologies of the samples were characterized via SEM (scanning electron microscopy) and TEM (transmission electron microscope). Thermal properties of composites were characterized using a TGA (Q5000 IR) from 50 to 700 °C at a heating rate of 10 °C/min under nitrogen atmosphere. The adhesive property tests were performed with the tensile machine (CMT, SANS) by the C-clamp according to the ASTM [20]. Rectangular specimens were heated from 25 to 90 °C at a rate of 1 °C/min to determine the dynamic-mechanical properties of composites using dynamic-mechanical analysis (Diamond DMA, Perkin-Elmer, USA) instrument in tension mode with a series of frequency from 0.01 Hz to 100 Hz. Through-plane diffusivity was measured by laser flash method on LFA457 (Netzsch). The in-plane diffusivity was performed on LFA467 (Netzsch). All thermal diffusivity measurements were performed at room temperature. Differential scanning calorimetry (DSC) was used to measure the specific heat capacity of the composites at room temperature. The thermal conductivity (k) was calculated by the following equation: $k = D \times \rho \times Cp$, where k, D, ρ and Cp are the thermal conductivity [W/m·K], thermal diffusivity (mm^2/s), density (kg/m^3), and specific heat capacity [J/kg·K]. Constant temperature resistance (12 V 60 °C 2–8 W) was mounted on the transformer (220 V to 12 V 60 W) to simulate the electronic devices. The operating temperature of the samples were monitored by CEM DT-980 thermal camera and the thermal images were captured.

3. Results and discussion

3.1. Surface modification of graphite flake

The procedure for modification of graphite flake by polydopamine was showed in Fig. 1. Ethanol was added into Tris-buffer solution to improve the dispersibility of graphite flake. On the other hand, ethanol could slow down the polymerization rate of dopamine in the Tris-buffer solution and prevent the aggregation of graphite flake with each other [21]. It was believed that substrates with conjugate structure such as graphene, h-BN, and graphite, which showed a strong π-π interaction with polydopamine [22,23]. Therefore, the similar hexagonal conjugate structure of graphite flake could be easily and efficiently modified by dopamine chemistry modification.

The morphologies of pristine and dopamine-treated graphite flake were observed by SEM characteristic. The pure graphite flake presented a smooth surface and became rough after polydopamine functionalization showed in Fig. 2, which indicated that the polydopamine layer was coated onto the particle surface [24].

TEM image further confirmed the successful modification of graphite flake by polydopamine. As showed in Fig. 3, a continuous, thin layer (ca. 25 nm) was observed on the surface of dopamine-treated graphite flake, indicating that the graphite flake was encapsulated by the polydopamine layer.

Fig. 4 (a) showed the significant differences between pristine and functionalized graphite flake in Raman spectra. Pristine graphite flake exhibited two characteristic peak at 1343 cm^{-1} and 1578 cm^{-1} which were attributed to the strong G band (E_{2g} mode) and weak D band scattering process [25,26]. Beside the intrinsic peak of pristine graphite flake, dopamine functionalized graphite flake showed some broad peaks at 1244, 1343, 1530 and 1643 cm^{-1}, which were assigned to catechol stretching vibration and deformation in the polydopamine structure [27]. The FT-IR spectrum of PDA@graphite showed the characteristic peaks in Fig. 4 (b), which could also be used to verify the existence of polydopamine. The wide peaks at 3676–3045 cm^{-1} and 1126 cm^{-1} which were attributed to the stretching vibration of O—H and C—O in PDA. The N—H shearing vibration of the amide group could be found at 1504 cm^{-1}. The vibration of phenolic C—O—H bending in polydopamine could be observed at 1382 cm^{-1} [22]. The characteristic peaks at 1504 cm^{-1} and 1650 cm^{-1} were corresponding to the C=C resonance vibration in aromatic ring of polydopamine and graphite, respectively [28,29].

Fig. 5 compared the thermal degradation behavior of pristine and

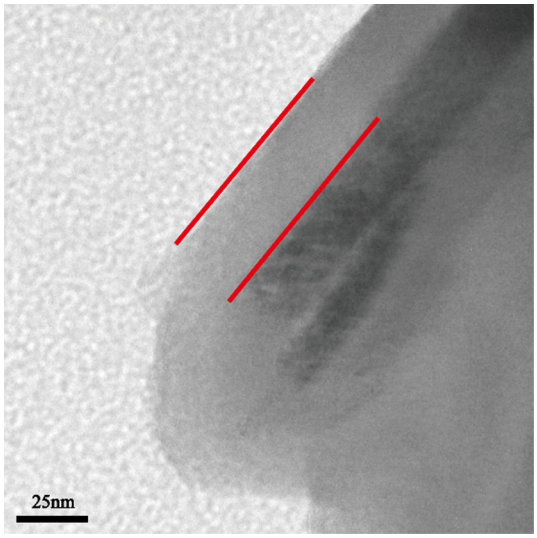

Fig. 3. TEM image of dopamine-treated graphite flake. (For interpretation of the references to colour in this figure legend, the reader is referred to the web version of this article.)

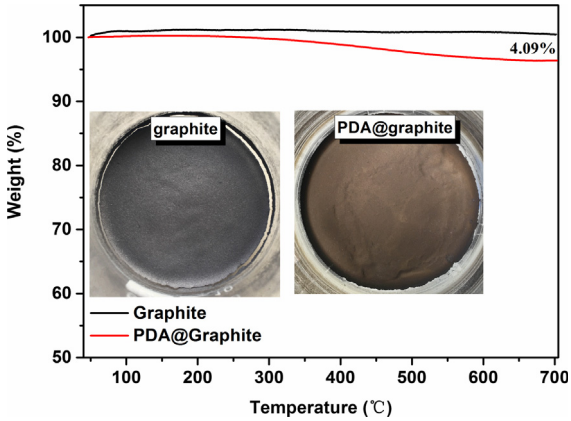

Fig. 5. Thermal degradation of pristine and dopamine-treated graphite flake with real images. (For interpretation of the references to colour in this figure legend, the reader is referred to the web version of this article.)

dopamine-treated graphite flake. Pristine graphite flake showed high thermal stability up to 700 °C without any decomposition. In contrast, dopamine-treated graphite flake began to degrade at about 250 °C and experienced major weight loss between 300 and 500 °C due to the decomposition of polydopamine molecules. Approximately 4.09 wt% polydopamine was attached to the graphite flake surface, which revealed by the weight loss during the pyrolysis procedure. Because of the formation of polydopamine thin layer on the graphite flake surface, the color of powder turned from black to gold as showed in Fig. 5 after modification.

3.2. Film formation of the composite film with aligned structure

Fig. 6 provided a visualized comparison on the dispersion of PDA@graphite aligned in polymer matrix via SEM images. The increased loading of filler decreased the smooth part (represented the polymer matrix Fig. S1) in Fig. 6 SEM images significantly. As we can see the red lines (represented the filler) in Fig. 6 (a), (b), and (c), an aligned stacking of PDA@graphite could be observed in the composite film. It was worth noting that the bending of fillers and some voids in the composite film, especially when filler loading was high. The main reason might due to the flexibility and interaction of PDA@graphite and we would explain this phenomenon by XRD measurement. Fig. 6 (d) presented the surface SEM images of the composite film and the illustration of the film formation process. The PDA@graphite filler stacked more closely with increasing the loading of filler, which would affect the properties of the composite film we would discuss follow. The amino groups on the surface of PDA@graphite would also participated in the curing process of the epoxy. The disappearance of the epoxy group meant that the completion of the curing process (Fig. S2). In order to further verify the structure of the composite film, XRD measurement was used to investigate the orientation degree of the filler PDA@graphite in the composite film.

The XRD patterns of the composite film provided additional support for the formation of the aligned structure (Fig. 7). Two different calculating methods were used to evaluate the degree of orientation. The (1 0 1) peaks at 2θ = 44.5° in the XRD patterns of the CER/PDA@graphite composites were much weaker than the (0 0 2) and (0 0 4) peaks at 2θ = 26.7° and 2θ = 54.6°. This phenomenon indicated the occurrence of orientation in the CER/PDA@graphite composites [30]. The orientation direction was parallel to the (0 0 2) crystal plane. The degree of orientation could be simply estimated by the ratio of (0 0 2) with (1 0 1) peaks. A high intensity ratio of (0 0 2) with (1 0 1) peaks implied a stronger orientation, suggesting that the aligned structure of the composites we obtained [31]. However, an interesting phenomenon was observed in Fig. 7 (a) that when we increased the content of PDA@graphite, the ratio of (0 0 2) and (1 0 1) peak decreased, which was contrary to prior reports [30]. In order to explain this phenomenon, we would evaluate the orientation degree of filler PDA@graphite in the composite film by the orientation function (*f*). And we could calculate

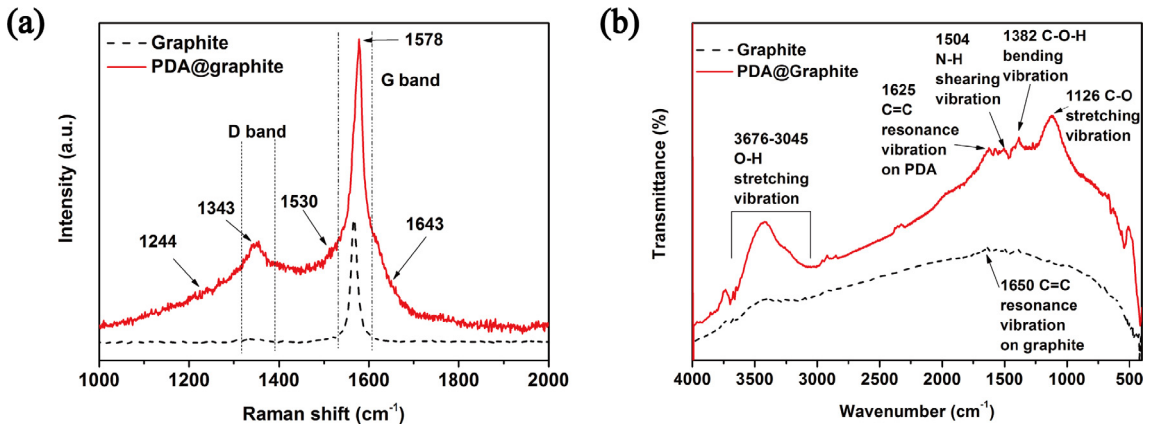

Fig. 4. Raman and FI-IR spectra of pristine and dopamine-treated graphite flake. (For interpretation of the references to colour in this figure legend, the reader is referred to the web version of this article.)

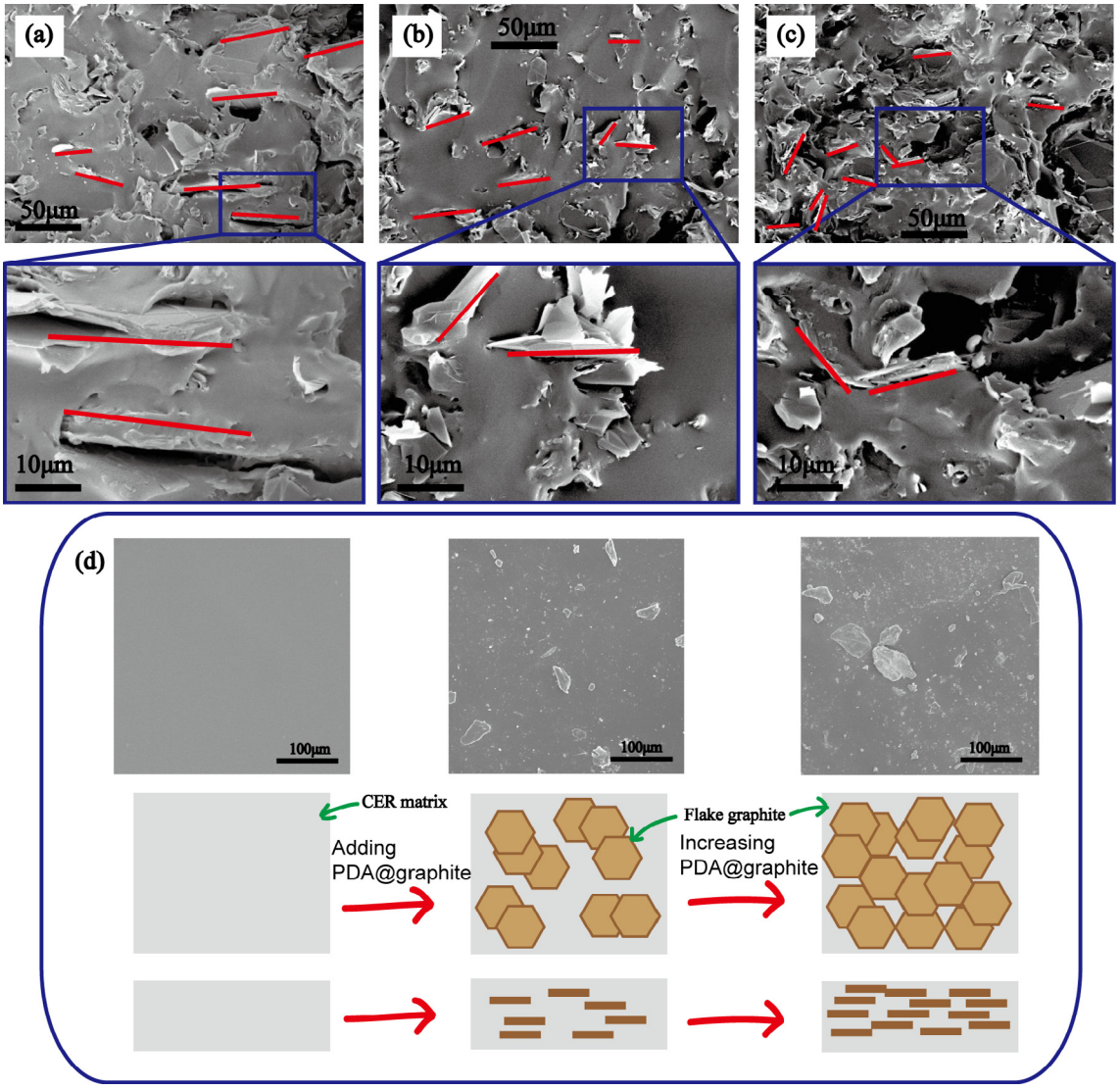

Fig. 6. (a), (b), (c) Cross-section SEM images, and (d) surface SEM images and illustration of the composite films with increasing the content of PDA@graphite. (For interpretation of the references to colour in this figure legend, the reader is referred to the web version of this article.)

the orientation function (f) by the following equations [32]:

$$f = (1-K)/(1 + 2K) \quad (1)$$

$$K = k \cdot I_{(002)}/I_{(101)} \quad (2)$$

where k is the normalization coefficient ~5.99 determined by the ratio intensity of (0 0 2) and (1 0 1) peak. Complete orientation of h-BN along in-plane direction in the composite film, which has $f = -0.5$.

We could find that the value of orientation function (f) increased slightly when we increased the content of filler (Fig. 7 (b)). However, we could find that the value of orientation function (f) was still very closer to −0.5, which meant that the higher orientation degree of filler PDA@graphite along the horizontal direction [32]. Therefore, the aligned filler played the main role in the composite film.

Above all, the overloaded PDA@graphite sheet limited their own movement during high-shear mixing preparing procedure, which increased the probability of dislocation and bending of the PDA@graphite sheets. The illustration model showed in Fig. 7 and the red line showed in Fig. 6 SEM images presented the visualized explanation and verification. In addition, the dislocation and bending of the PDA@graphite sheets might also introduce the voids in the composite film.

3.3. The mechanical properties of the composite film

Fig. 8 presented the storage modulus (E′), loss modulus (E″), Cole-cole plots of storage modulus versus loss modulus, and complex viscosity at 43 °C for the all samples. Dynamic mechanical analysis (DMA) measurement has been widely used to investigate the microstructure-performance relationship of materials, and especially, it provides not only the information about viscoelastic behavior but also the microstructure information on fillers in the composites. As we known that if a plateau was observed in the storage modulus curves at low frequencies, we could believe that a network-like structure of fillers formed in the composites, because the composites exhibited more apparent elastic characteristic, namely, the storage modulus exhibited relatively lower dependence on shear frequency [33]. When we increased the loading of PDA@graphite, an apparent plateau at low frequency range could be observed that E′ changed slightly with increasing frequency. This phenomenon indicated that the solid-like viscoelastic behavior induced by the greatly restrained long-range molecular chain motion. Such a phenomenon was generally induced by the presence of filler stacked structure [33]. This could be further investigated from the variations of Cole-cole plots of E′ versus E″. For the composites, the increase of E′ was higher than the increase of E″ with increasing filler loading. In addition,

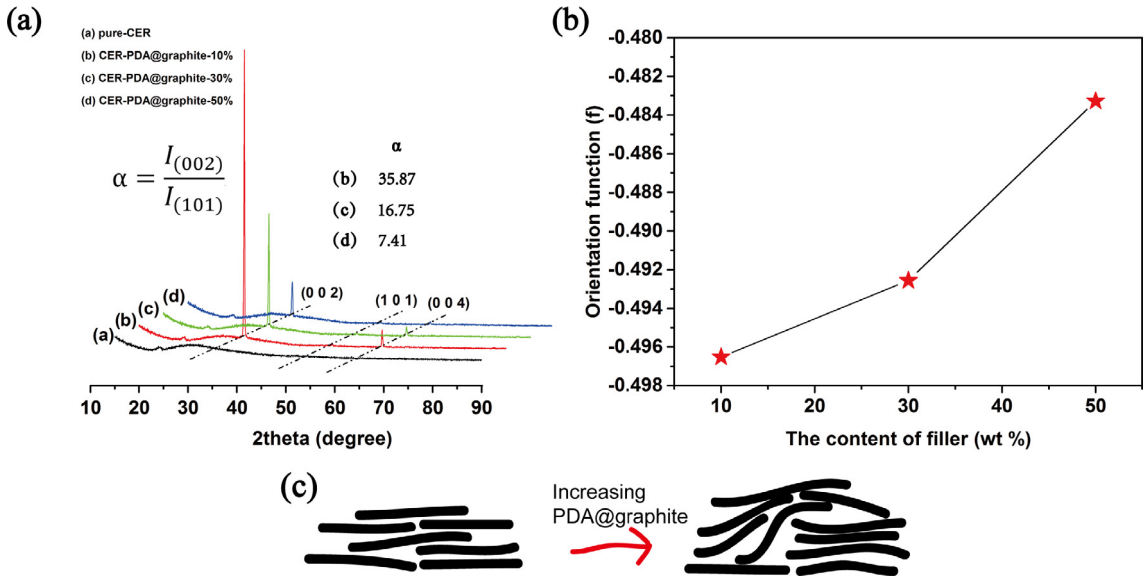

Fig. 7. (a) the XRD patterns of pure CER matrix and CER/PDA@graphite composites; (b) the orientation function (*f*) of the composite film; (c) the illustration model of fillers in the composite film. (For interpretation of the references to colour in this figure legend, the reader is referred to the web version of this article.)

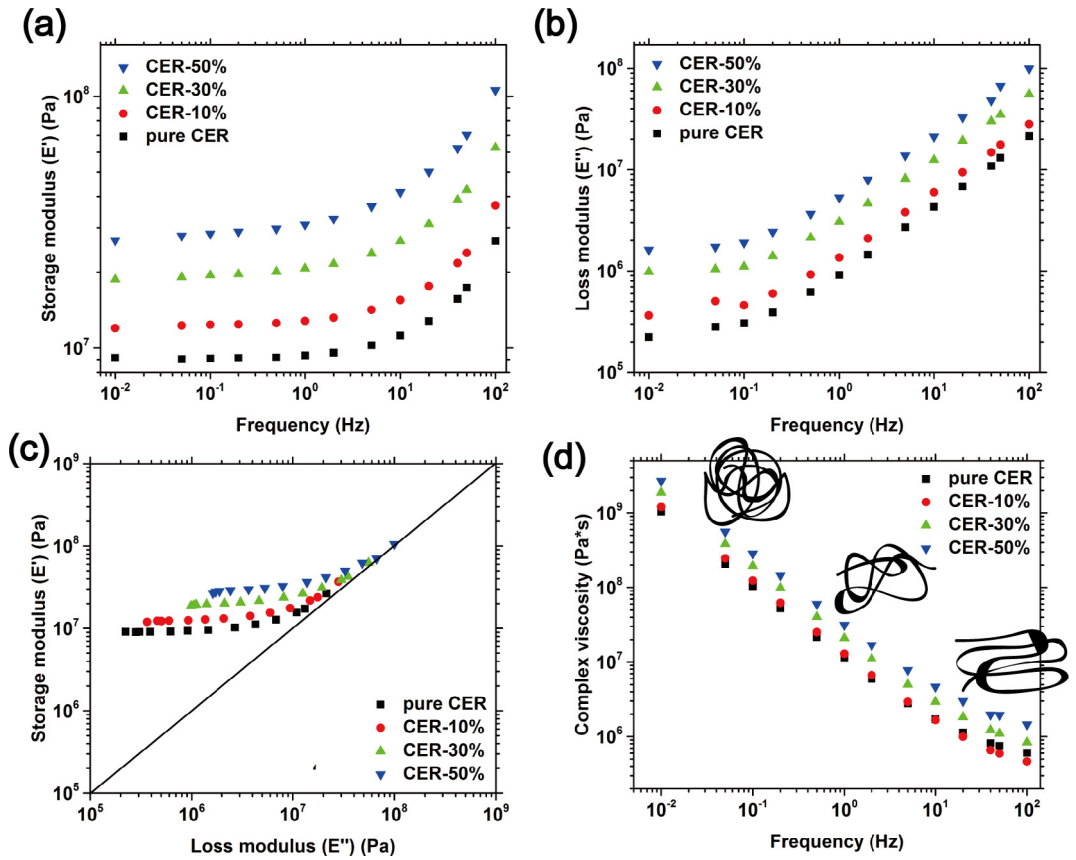

Fig. 8. Viscoelastic behavior of all the samples as indicated in the graphs (at 43 °C), (a) Storage modulus (E′), (b) loss modulus (E″), (c) Cole-cole plots of storage modulus versus loss modulus, (d) complex viscosity with the model for viscosity of polymer chains with changing the frequency.

a deviation from a linear relationship between E′ and E″ was obtained, which represented the presence of the filler stacked network structure in the composites [34]. Especially, when we increased the loading of filler, the density of aligned structure became higher. The frequency-dependence of η^* reflected the molecular rearrangement (entanglement/disentanglement) on timescale in response to both small-deformation and large-deformation perturbation. In Fig. 8 (d), complex viscosity decreased with increasing frequency, the polymer chain in CER/PDA@graphite composites became disentanglement from entanglement. In addition, the loading of filler also restricted the movement of the polymer chain in the composites due to the bending of fillers showed in Fig. 6 when the loading of filler was high [35].

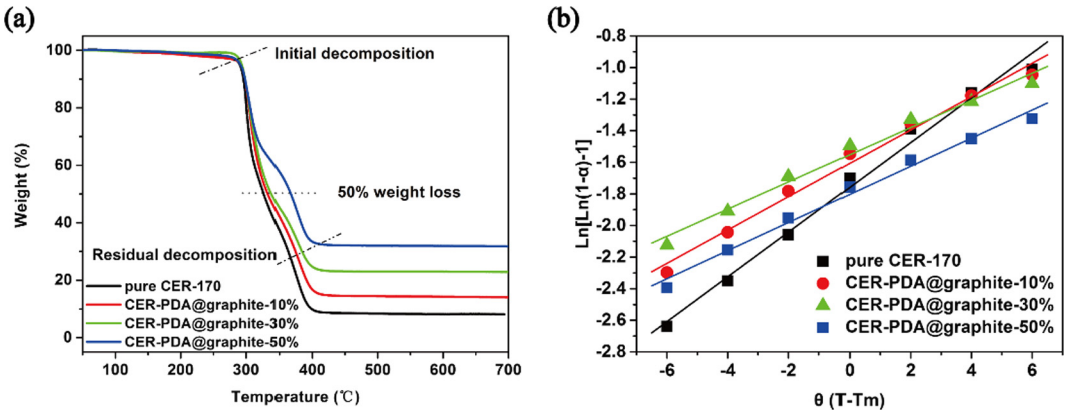

Fig. 9. (a) TGA curves of composites and (b) the plots of $\ln[\ln(1-\alpha)^{-1}]$ versus θ via Horowitz-Metzger method. (For interpretation of the references to colour in this figure legend, the reader is referred to the web version of this article.)

Table 1
Thermal stability of the composites obtained from TGA curves.

Filler	$A^*{\cdot}K^*$	T_{d50} (°C)	PDT (°C)	IPDT (°C)	E_t (kJ/mol)	R^2
Pure-CER	0.581	326.82	299.23	423.45	385.75	0.987
CER-PDA@graphite-10 wt%	0.707	333.08	304.07	510.26	292.44	0.985
CER-PDA@graphite-30 wt%	0.948	338.39	305.48	673.88	239.42	0.979
CER-PDA@graphite-50 wt%	1.272	367.15	303.14	897.37	245.76	0.986

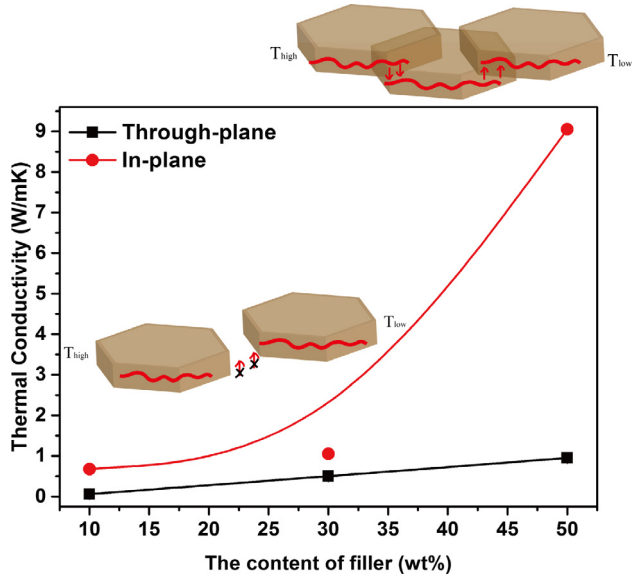

Fig. 10. Thermal conductivity vs PDA@graphite content in CER/PDA@graphite composites. (Note the error bars assimilated into the markers, due to the small measurement errors.) (For interpretation of the references to colour in this figure legend, the reader is referred to the web version of this article.)

3.4. Thermal stability of the composites

Fig. 9 (a) showed the thermo-gravimetric analyses of the composite film under nitrogen atmosphere. The loading of PDA@graphite influenced the thermal stability of the polymer matrix. At the initial decomposition stage, the difference of the temperature is negligible. However, the temperature at 50 wt% weight loss (T_{d50}) increased significantly when we increased the filler content. The platelet-liked filler enhanced the thermal stability of the composites due to the aligned stacking of the filler, which hindered the diffusion volatile decomposition parts in the composite film. Except for the decomposition hindering effect of the 2D thermal conductivity filler, we also had to consider the thermal conductivity of the filler, which might accelerate the decomposition (the decomposition accelerating effect) [36].

The mechanism of thermal decomposition were investigated by thermodynamic/kinetics analysis through TGA. Firstly, we calculated the integral procedural decomposition temperature (IPDT) as the kinetic parameters based on Doyle's proposition by following equations according to the TGA test [37,38]:

$$\mathrm{IPDT} = A^*{\cdot}K^*{\cdot}(T_f - T_i) + T_i \tag{3}$$

$$A^* = (A_1 + A_2)/(A_1 + A_2 + A_3) \tag{4}$$

$$K^* = (A_1 + A_2)/A_1 \tag{5}$$

where A^* was the area ratio between the total experimental curve and the total TGA curve; K^* represented the coefficient of A^*; T_i and T_f were the initial experimental temperature and final experimental temperature, respectively. The A_1, A_2, and A_3 were the area of the three regions dividing the TGA curve (Fig. S3). As we can see in Table 1. The IPDT is usually used to characterize the volatile parts in composites, therefore, we used it to estimate the inherent thermal stability of polymer composites [39]. The IPDT of pure cycloaliphatic epoxy (pure-CER) is 423.45 °C, and the value of the composites increased with improving the filler PDA@graphite content, which indicating the enhancement of the thermal stability.

Another important parameter was the activation energy (E_t) of decomposition which was calculated from TGA curves by integral method of Horowitz-Metzger, according to Eq. (8) [40–42].

$$\ln[\ln(1-\alpha)^{-1}] = \frac{E_t}{RT_{max}^2}\theta \tag{6}$$

where α was the fraction of sample decomposed; T_{max} was decomposition temperature at the maximum weight loss rate; E_t represented the activation energy for decomposition; θ was the difference between decomposition temperature T and T_{max} defined as $\theta = T - T_{max}$; R was the real gas constant (8.314 J/(mol·K)).

Fig. 9 (b) presented the plots of $\ln[\ln(1-\alpha)^{-1}]$ versus θ. The activation energy (E_t) of decomposition was calculated by fitting the slope and showed in Table 1. Interestingly, the values of E_t of the composites were lower than pure cycloaliphatic epoxy (pure-CER) meant that only less heat energy would decompose the composites. Therefore, the loading of filler PDA@graphite accelerated the decomposition and decreased the thermal stability of the composites. In addition, we could find that the values of E_t increased slightly when the content of filler

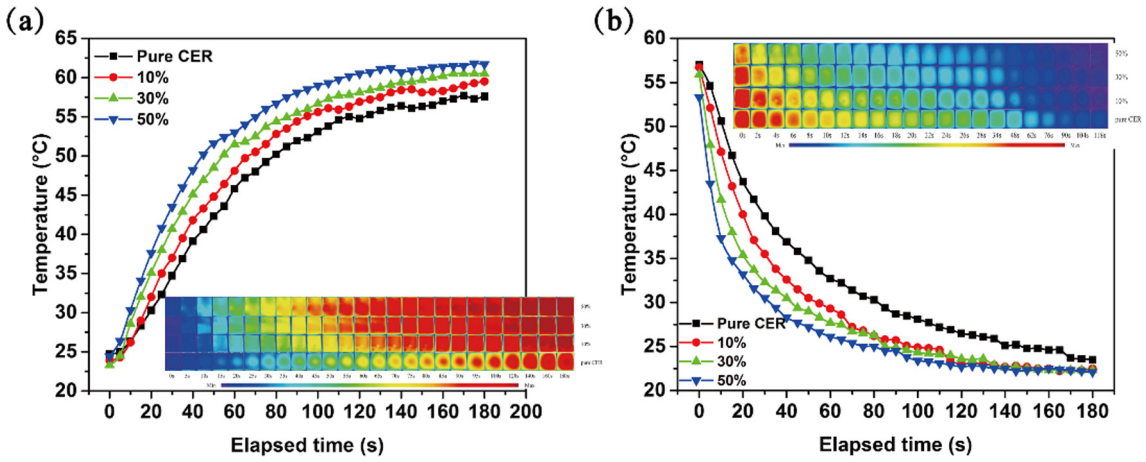

Fig. 11. Thermal transport evolution of (a) heating and (b) cooling with different PDA@graphite content in CER/PDA@graphite composites. (For interpretation of the references to colour in this figure legend, the reader is referred to the web version of this article.)

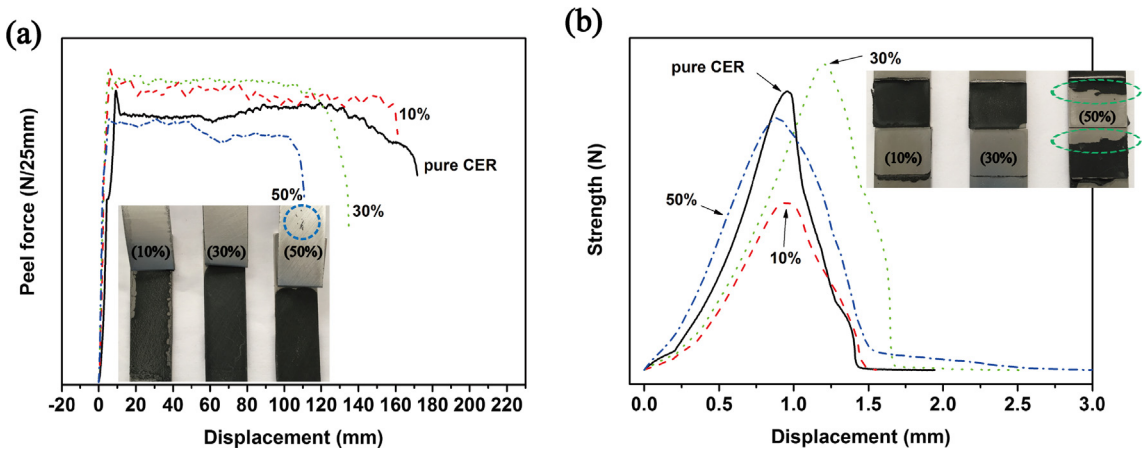

Fig. 12. The adhesive properties of (a) 180°-peel strength and (b) shear strength. (For interpretation of the references to colour in this figure legend, the reader is referred to the web version of this article.)

arrived at 50 wt%. The main reason might be that the decomposition hindering effect of the 2D thermal conductivity filler which still played a main role during the decomposition process. Therefore, the balance between that two facts (IPDT and E_t) resulted in the complex TGA curves showed in Fig. 9.

3.5. Thermal conductivity of the composite film

Because of the geometric factor of graphite flake, the thermal pathways formed along the horizontal direction. The in-plane orientated CER/PDA@graphite composites demonstrated a higher thermal conductivity than those on the through-plane direction. The contacting of the filler could also be proved by the result we discussed in the XRD measurement showed in Fig. 7 (c). And the flexibility and bending of the filler PDA@graphite reduced the thermal resistance of contact between the fillers. Fig. 10 presented the thermal conductivity vs PDA@graphite content in CER/PDA@graphite composites. The PDA@graphite largely improved the thermal conductivity at the value of 9.053 W/m·K with 50 wt% PDA@graphite. The through-plane thermal conductivity of the composites also had slight improvement due to the closer stacking of the filler. In addition, the dislocation and bending of the filler also provided some thermal pathways along the vertical direction (Fig. 7 (c)).

The samples of composites and pure CER matrix were placed on the same heating and cooling stage. The temperature distribution on them was captured as a function of the elapsed time and showed by the color in Fig. 11. On heating stage, the thermal transport speed became faster with the filler content increasing, which meaning the thermal transport ability of CER matrix was improved by the thermal conductive filler. The final stable temperature also became higher owing to the closed stacking structure on the through-plane direction and some thermal pathways along the vertical direction when the loading of filler was increased. Therefore, for the cooling stage, the more loading of filler, the faster cooling speed had.

3.6. The adhesive property of the composite film

The 180°-peel strength of the CER/PDA@graphite composite film was presented in Fig. 12 (a). The loading of filler increased the peel strength of the composite film due to the aligned stacking structure of filler which restricted the breaking of the polymer matrix [43]. However, a significant decrease in performance happened after the filler content arrived at 50 wt%. The main reason might be that the bending of the filler and the voids in the composites reduced the stability of the aligned stacking structure of filler and then reduced the peel strength of the composite film. Fig. 12 (b) showed the shear strength of the composite film. The filler content of 30 wt% enhanced the polymer matrix. For the same reason, overloading of filler broke the cohesive strength and cohesive failure happened. The real images presented in Fig. 12 showed the process directly. Although, the loading of PDA@graphite reduced the peel strength, the adhesive performance was still good enough to achieve the practical application.

4. Conclusion

Dopamine chemistry was used to achieve the facile modification of graphite flake via forming a polydopamine (PDA) shell on the surface in a solvent-free aqueous condition. The strong π-π interaction between the hexagonal structural graphite flake and aromatic dopamine molecules ensured the effective modification. The successful preparation of PDA@graphite increased the adhesive of filler and matrix via hydrogen bond and covalent bond from the PDA coating. The XRD measurement and dynamic mechanical analysis (DMA) were used to study the relationship between microstructure and performance successfully. The procedure of thermal decomposition was explained by calculating the integral procedural decomposition temperature (IPDT) and activation energy (E_t). The prepared CER/PDA@graphite exhibited excellent performance such as in-plane thermal conductivity, adhesive properties and thermal stability, which could be used as a promising thermal interface material in thermal management for electronic and photonic applications.

Acknowledgements

The authors would like to acknowledge the financial support from National Key R&D Program of China (No. 2017YFB0406200) and the Strategic Priority Research Program of the Chinese Academy of Sciences (Grant No. XDA13040505).

Appendix A. Supplementary material

Supplementary data associated with this article can be found, in the online version, at http://dx.doi.org/10.1016/j.compositesa.2018.02.033.

References

[1] Shahil KMF, Balandin AA. Graphene-multilayer graphene nanocomposites as highly efficient thermal interface materials. Nano Lett. 2012;12(2):861–7.
[2] Wong CP, Moon KS, Li Y. Nano-bio- electronic, photonic and MEMS packaging. US: Springer; 2010.
[3] Prasher RS, Narasimhan S. Nano and micro technology-based next-generation package-level cooling solutions. Intel Technol J 2005;09(4):p285.
[4] Kim P, Shi L, Majumdar A, McEuen PL. Thermal transport measurements of individual multiwalled nanotubes. Phys Rev Lett 2001;87(21):215502.
[5] Ghosh S, Calizo I, Teweldebrhan D, Pokatilov EP, Nika DL, Balandin AA, et al. Extremely high thermal conductivity of graphene: prospects for thermal management applications in nanoelectronic circuits. Appl Phys Lett 2008;92(15):151911.
[6] Tian X, Itkis ME, Bekyarova EB, Haddon RC. Anisotropic thermal and electrical properties of thin thermal interface layers of graphite nanoplatelet-based composites. Sci Rep 2013;3:1710.
[7] Zhang H, Chen X, Jho Y-D, Minnich AJ. Temperature-dependent mean free path spectra of thermal phonons along the c-axis of graphite. Nano Lett 2016;16(3):1643–9.
[8] Chen Z, Jang W, Bao W, Lau CN, Dames C. Thermal contact resistance between graphene and silicon dioxide. Appl Phys Lett 2009;95(16):161910–3.
[9] Tian X, Itkis ME, Haddon RC. Application of hybrid fillers for improving the through-plane heat transport in graphite nanoplatelet-based thermal interface layers. Sci Rep 2015;5:13108.
[10] Zheng R, Gao J, Wang J, Feng S-P, Ohtani H, Wang J, et al. Thermal percolation in stable graphite suspensions. Nano Lett 2012;12(1):188–92.
[11] Zhou Y, Yao Y, Chen C-Y, Moon K, Wang H, Wong C-P. The use of polyimide-modified aluminum nitride fillers in AlN@PI/Epoxy composites with enhanced thermal conductivity for electronic encapsulation. Sci Rep 2014;4:4779.
[12] Yu J, Huang X, Wang L, Peng P, Wu C, Wu X, et al. Preparation of hyperbranched aromatic polyamide grafted nanoparticles for thermal properties reinforcement of epoxy composites. Polym Chem 2011;2(6):1380–8.
[13] Yu J, Huang X, Wu C, Wu X, Wang G, Jiang P. Interfacial modification of boron nitride nanoplatelets for epoxy composites with improved thermal properties. Polymer 2012;53(2):471–80.
[14] Peng W, Huang X, Yu J, Jiang P, Liu W. Electrical and thermophysical properties of epoxy/aluminum nitride nanocomposites: effects of nanoparticle surface modification. Compos A Appl Sci Manuf 2010;41(9):1201–9.
[15] Yu A, Ramesh P, Itkis ME, Elena Bekyarova A, Haddon RC. Graphite nanoplatelet−epoxy composite thermal interface materials. J Phys Chem C 2007;111(21):084504-4.
[16] Feng T, Ruan X. Prediction of spectral phonon mean free path and thermal conductivity with applications to thermoelectrics and thermal management: a review. J Nanomater 2014;2014(3):1–25.
[17] Shen X, Wang Z, Wu Y, Liu X, He Y-B, Kim J-K. Multilayer graphene enables higher efficiency in improving thermal conductivities of graphene/epoxy composites. Nano Lett 2016;16(6):3585–93.
[18] Shen H, Guo J, Wang H, Zhao N, Xu J. Bioinspired modification of h-BN for high thermal conductive composite films with aligned structure. ACS Appl Mater Interfaces 2015;7(10):5701–8.
[19] Ahn HJ, Eoh YJ, Park SD, Kim ES. Thermal conductivity of polymer composites with oriented boron nitride. Thermochim Acta 2014;590:138–44.
[20] Kobayashi M, Takahara A. Environmentally friendly repeatable adhesion using a sulfobetaine-type polyzwitterion brush. Polym Chem 2013;4(18):4987–92.
[21] Yan J, Yang L, Lin M-F, Ma J, Lu X, Lee PS. Polydopamine spheres as active templates for convenient synthesis of various nanostructures. Small 2013;9(4):596–603.
[22] He Y, Wang J, Zhang H, Zhang T, Zhang B, Cao S, et al. Polydopamine-modified graphene oxide nanocomposite membrane for proton exchange membrane fuel cell under anhydrous conditions. J Mater Chem A 2014;2(25):9548–58.
[23] Thakur VK, Yan J, Lin M-F, Zhi C, Golberg D, Bando Y, et al. Novel polymer nanocomposites from bioinspired green aqueous functionalization of BNNTs. Polym Chem 2012;3(4):962–9.
[24] Wu H, Kessler MR. Multifunctional cyanate ester nanocomposites reinforced by hexagonal boron nitride after noncovalent biomimetic functionalization. ACS Appl Mater Interfaces 2015;7(10):5915–26.
[25] Lucchese MM, Stavale F, Ferreira EHM, Vilani C, Moutinho MVO, Capaz RB, et al. Quantifying ion-induced defects and Raman relaxation length in graphene. Carbon 2010;48(5):1592–7.
[26] Tuinstra F, Koenig JL. Raman spectrum of graphite. J Chem Phys 2003;53(3):1126–30.
[27] Ku SH, Lee JS, Park CB. Spatial control of cell adhesion and patterning through mussel-inspired surface modification by polydopamine. Langmuir 2010;26(19):15104–8.
[28] Wang J, Xiao L, Zhao Y, Wu H, Jiang Z, Hou W. A facile surface modification of Nafion membrane by the formation of self-polymerized dopamine nano-layer to enhance the methanol barrier property. J Power Sources 2009;192(2):336–43.
[29] Su Z, Wang H, Tian K, Xu F, Huang W, Tian X. Simultaneous reduction and surface functionalization of graphene oxide with wrinkled structure by diethylenetriamine (DETA) and their reinforcing effects in the flexible poly(2-ethylhexyl acrylate) (P2EHA) films. Compos A Appl Sci Manuf 2016;84:64–75.
[30] Yuan G, Li X, Dong Z, Westwood A, Cui Z, Cong Y, et al. Graphite blocks with preferred orientation and high thermal conductivity. Carbon 2012;50(1):175–82.
[31] Zhou S-x, Zhu Y, Du H-d, Li B-h, Kang F-y. Preparation of oriented graphite/polymer composite sheets with high thermal conductivities by tape casting. New Carbon Mater 2012;27(4):241–9.
[32] Tanimoto M, Yamagata T, Miyata K, Ando S. Anisotropic thermal diffusivity of hexagonal boron nitride-filled polyimide films: effects of filler particle size, aggregation, orientation, and polymer chain rigidity. ACS Appl Mater Interfaces 2013;5(10):4374–82.
[33] Sumita M, Sakata K, Asai S, Miyasaka K, Nakagawa H. Dispersion of fillers and the electrical conductivity of polymer blends filled with carbon black. Polym Bull 1991;25(2):265–71.
[34] Khare RA, Bhattacharyya AR, Kulkarni AR, Saroop M, Biswas A. Influence of multiwall carbon nanotubes on morphology and electrical conductivity of PP/ABS blends. J Polym Sci, Part B: Polym Phys 2008;46(21):2286–95.
[35] Morris ER, Nishinari K, Rinaudo M. Gelation of gellan – a review. Food Hydrocolloids 2012;28(2):373–411.
[36] Su Z, Wang H, Ye X, Tian K, Huang W, Guo Y, et al. Non-covalent poly (2-ethylhexyl acrylate) (P2EHA)/functionalized graphene/h-boron nitride flexible composites with enhanced adhesive and thermal conductivity by a facilitated latex approach. Compos A Appl Sci Manuf 2017;99:176–85.
[37] Park S-J, Cho M-S. Thermal stability of carbon-MoSi2-carbon composites by thermogravimetric analysis. J Mater Sci 2000;35(14):3525–7.
[38] Goyat MS, Ray S, Ghosh PK. Innovative application of ultrasonic mixing to produce homogeneously mixed nanoparticulate-epoxy composite of improved physical properties. Compos A Appl Sci Manuf 2011;42(10):1421–31.
[39] Kuan C-F, Chen W-J, Li Y-L, Chen C-H, Kuan H-C, Chiang C-L. Flame retardance and thermal stability of carbon nanotube epoxy composite prepared from sol–gel method. J Phys Chem Solids 2010;71(4):539–43.
[40] Wu S-Y, Huang Y-L, Ma C-CM, Yuen S-M, Teng C-C, Yang S-Y. Mechanical, thermal and electrical properties of aluminum nitride/polyetherimide composites. Compos A Appl Sci Manuf 2011;42(11):1573–83.
[41] Zhang Y, Ge X, Deng F, Li M-C, Cho UR. Fabrication and characterization of rice bran carbon/styrene butadiene rubber composites fabricated by latex compounding method. Polym Compos 2015;16:101–13.
[42] Gonsalves KE, Chen X, Baraton M-I. Mechanistic investigation of the preparation of polymer/ceramic nanocomposites. Nanostruct Mater 1997;9(1):181–4.
[43] Su Z, Wang H, Xu F, Tian K, Wu J, Tian X-Y. Tunable composite architecture and homogeneous dispersion of charged SiO_2 in polymer matrix assisted by Poly(2-Ethylhexyl acrylate) (P2EHA) latex prepared by self-assembly through electrostatic interaction. RSC Adv 2016;6(7):5621–30.